Applied Surface Science 588 (2022) 152896

Contents lists available at ScienceDirect

Applied Surface Science

journal homepage: www.elsevier.com/locate/apsusc

Full Length Article

Reduction of thermally grown single-phase CuO and Cu_2O thin films by in-situ time-resolved XRD

Yeliz Unutulmazsoy [1,*], Claudia Cancellieri [1,*], Luchan Lin [2], Lars P.H. Jeurgens

Empa, Swiss Federal Laboratories for Materials Science and Technology, Laboratory for Joining Technologies and Corrosion, Switzerland

ARTICLE INFO

Keywords:
Reduction kinetics
Real time XRD
Nanoporous structures
Thin film oxidation
Oxide thin film reduction

ABSTRACT

Copper oxide is used as a catalyst or catalyst precursor in chemical reactions that involve hydrogen as a reactant or a product. Controlled reduction and therefore known reduction kinetics of well-defined Cu-oxides in hydrogen is a key issue for the activation of oxide catalysts as well as for other technological fields such as gas sensing. The kinetics and mechanisms of reduction of single-phase CuO and Cu_2O films in 5 vol% H_2/Ar were investigated by in-situ real time synchrotron-based X-ray diffraction measurements. To this end, the incubation time, the CuO → Cu_2O and Cu_2O → Cu phase transformation rates, as well as the microstructure and strain state of the evolving Cu, CuO and Cu_2O phases were studied during the reduction. Highly porous Cu and Cu-oxides scaffolds were obtained by alternating oxidation and reduction steps, which can be envisaged for a wealth of applications in the fields of catalysis, batteries, water treatment and biomedical applications.

1. Introduction

The reduction of oxides plays an eminent role in heterogeneous catalysis,[1-5] but is also essential in the numerous other application fields, such as nanopaste sintering for joining [6-8], corrosion [9], 3D-printing of metals via reduction of printed or extruded oxide nano-powders [10,11], batteries [12-14], and gas sensing [15]. Independent of the targeted application, the kinetics of the oxide reduction process is generally rate-limited by the reaction of the reducing agent with the oxide surface, generating oxygen vacancies in the oxide sublattice [1,2,16-18].

Fundamental knowledge on the kinetics and mechanism of the reduction of CuO and/or Cu_2O in H_2 gas mixtures is of particular interest for heterogeneous catalysis [3], gas sensing [15] and nanopaste sintering [6]. The studies on the reduction of copper oxide by hydrogen dates back to the 18th century and concluded that the reduction of CuO to Cu is preceded by an "incubation" period where there is no perceptible reaction [19]. Ever since, the incubation time for the reduction of CuO and Cu_2O in hydrogen has been a topic of many studies. The length of the incubation period for the reduction of CuO increases with decreasing the temperature and decreasing hydrogen partial pressure [1,2,19,20]. Initially, the incubation time was attributed to the time required to form stable metallic Cu phase [20]. More recent studies have concluded that the incubation time is associated with the time required to generate sufficiently high concentration of oxygen vacancies in the oxide (sub) surface region to catalyse the adsorption and dissociation of H_2 [1,2,18].

For practical and technological reasons, the reduction kinetics of CuO and/or Cu_2O in H_2 and/or CO gas mixtures have been mostly studied on (sub)micron-sized powder mixtures [1,2,6,8,21], pressed powder pellets [22], as well as nanoaggregates such as nanoparticles, nanowires, rods, and etc [23,24]. Such micro- and/or nano-scaled assemblies typically possess relatively broad size and shape distributions of the principle building blocks (e.g. particles, rods, platelets) and their aggregates, which may lead to very different surface morphologies, defect structures and CuO-to-Cu_2O phase fractions in the as-prepared state [21,25,26]. Unfortunately, the size and shape distributions of the studied powders in their as-prepared state are often not specified [1,2,22]. The large spread in CuO/Cu_2O powder and aggregate characteristics has resulted in many contradictory findings on the incubation times, reaction rates and phase transformation sequence for the oxide reduction processes. Foremost, three different phase transformation sequences for the reduction of CuO in H_2 have been reported. (i) The complete full transformation sequence CuO → Cu_4O_3 → Cu_2O → Cu has only been observed for the reduction of CuO in a hydrogen plasma

* Corresponding authors at: Leibniz Institute for Surface Engineering, Permoserstrasse 15, 04318 Leipzig, Germany (Yeliz Unutulmazsoy).
E-mail addresses: yeliz.unutulmazsoy@iom-leipzig.de (Y. Unutulmazsoy), claudia.cancellieri@empa.ch (C. Cancellieri).
[1] Equally contributed to this work.
[2] School of Materials Science and Engineering, Shanghai Jiaotong University, Shanghai 200240, China.

https://doi.org/10.1016/j.apsusc.2022.152896
Received 30 December 2021; Received in revised form 17 February 2022; Accepted 20 February 2022
Available online 26 February 2022

(containing atomic hydrogen) [22]. The reduction of CuO in H_2 requires dissociative chemisorption of H_2 molecules on the oxide surface; in this case, both (ii) the direct CuO → Cu transformation (without the formation of intermediate Cu_2O or Cu_4O_3 phases) [1,2], (iii) as well the sequential reduction CuO → Cu_2O → Cu has been reported [23,27,28]. Previous CuO reduction studies have mainly focused on the phase transformation sequence and the detection of intermediate oxide species [1,2,23,24], but rarely on the kinetics of the reduction process. Since the reduction kinetics will depend largely on the undefined powder characteristics, it hinders a direct comparison of reduction rates between different studies on powders and/or aggregates.

In the present study, dense polycrystalline single-phase CuO and Cu_2O thin films with thicknesses in the range of roughly 80 to 530 nm were prepared by a controlled thermal oxidation of thin Cu films at different temperatures. A detailed study on the oxidation kinetics of thin Cu films can be found elsewhere [29]. The single-phase CuO and Cu_2O films were reduced in 5 vol% H_2/Ar gas mixtures at 300 °C, while monitoring the incubation time and the subsequent phase transformation sequence (either CuO → Cu_2O or Cu_2O → Cu) by in-situ time-resolved XRD at the synchrotron. The combination of a high intensity of synchrotron radiation with a custom-designed furnace with full atmospheric control makes it possible to conduct sub-minute, time-resolved XRD measurements under a wide variety of temperatures and atmospheric conditions. In addition, the average CuO, Cu_2O and/or Cu grain sizes, as well as the strain evolution, during the reduction process were resolved from the large data sets, which have not been performed and investigated in such detail up to date. After complete reduction, the initially dense and smooth Cu-oxide films (as obtained by thermal oxidation) were converted into highly (nano)porous metallic Cu films with a high specific surface area, which can be envisaged for a wide range of applications in the fields of catalysis, batteries, water treatment and biomedical applications .

2. Experimental

50, 150 and 300 nm thick initial Cu films were grown on 10 × 10 mm^2 sapphire substrates (single crystalline α-Al_2O_3 - C(0001), supplied by *CrysTec*) in an ultra-high vacuum chamber (<1 × 10^{-8} mbar) from a Cu target (99.99%) at room temperature by DC magnetron sputtering (80 W, 0.5 Pa Ar). Prior to deposition, the substrates were ultrasonically cleaned in acetone and ethanol. Then, RF-plasma cleaning was performed inside the deposition chamber directly before the deposition step.

Real-time high-temperature synchrotron XRD measurements during oxidation of the metal films, as well as upon subsequent reduction of the oxidized films, were performed in the temperature range between 200 and 400 °C at the material science beamline (MS-X04SA) at the Swiss Light Source (SLS) in Paul Scherrer Institute (PSI), Villigen, Switzerland. The MS-X04SA beamline is designed to provide a high-intensity X-ray beam with a tunable wavelength in the energy range of 5–40 keV. The time resolved X-ray diffraction data during oxidation and reduction were collected from the powder diffraction branch using a photon energy of 25.1936 keV at 401.1 mA ($\lambda = 0.4921$ Å) in transmission mode with a two-dimensional detector (*PILATUS*, *DECTRIS*). A detailed description of the beamline setup and the detector is given elsewhere [30]. The beamline setup was equipped with a custom-designed compact furnace for in-situ heating in a controlled atmosphere (supplied by *IRELEC*) during the XRD measurements, employing a beam size of 200 × 150 μm^2. The atmosphere (the partial pressures) in the furnace during oxidation in O_2(g)/Ar(g) and reduction in H_2(g)/Ar(g) were precisely controlled by mass flow controllers keeping the total pressure around 1 bar. After mounting each new sample on the sample stage (with the substrate side facing the incident X-ray beam and the thin film facing the detector), the furnace was pumped down to 1 × 10^{-4} mbar for several minutes. Then, the furnace was heated up to the desired oxidation or reduction temperature with a heating rate of 10 K/min in Ar atmosphere (>99.9999% with a constant flow rate < 200 ml/min). The temperature was regulated through an *Eurotherm* 3208 temperature controller with the type-K thermocouple in intimate contact with the sample stage, close to the clamped sample. As soon as the targeted temperature was reached, the atmosphere was switched to the selected gas mixture for oxidation or reduction. Successive diffraction patterns were recorded in 2theta range of 0-30° with a time interval of 40 s. The oxidation and reduction steps were performed on the same sample, consecutively without any interruption. To this end, the Cu films were first fully oxidized to a single phase at a given oxidation temperature. Then, the oxidizing atmosphere was switched back to Ar to change the targeted isothermal reduction temperature. After reaching the desired temperature in Ar for reduction purposes, the atmosphere was switched to a reducing atmosphere of 5 vol% H_2/Ar mixture (see Fig. 1). All reduction experiments were performed at the same conditions; at 300 °C in 5 vol% H_2/Ar atmosphere, while recording the diffraction patterns in the 2theta range of 0-30° with a time interval of 40 s.

High-resolution scanning electron microscopy (SEM, *Hitachi S-4800*) was applied for planar and cross-sectional analysis of the oxidized and reduced films. A cross section of the metallic Cu film and reduced Cu-oxide film were prepared by focused ion beam (FIB) milling under the vision of scanning electron microscopy (SEM) using a *FEI Helios Nanolab Dual Beam*. Before ion milling, protective Pt layers were pre-deposited on the film surfaces.

The individual sets of measured diffractograms for each experiment were obtained as a function of time by integrating each successively captured image on the 2D detector (correcting for the mask lattice with zero intensity in between neighboring detector segments and previously calibrated for the 2theta positions). The obtained series of integrated 2theta spectra were assigned to the monitored eurotherm temperatures (using their respective time stamps) and the diffractograms as a function of time is further processed using a Matlab code. The selected peaks for data analysis based on the highest intensity of Cu, Cu_2O or CuO reflections were clearly visible (no overlapping of the peaks), so a polynomial background (of the third degree) was subtracted over the selected 2theta range. Next, the corresponding position, full width half maximum (FWHM) and integrated peak area of the peak was extracted from the background corrected diffractogram. The average strain, ε, has been derived for each phase (Cu, CuO and Cu_2O) at high temperature from the respective (1 1 1) reflection according to

$$\varepsilon = \left[d_{(111)} - d^0_{(111)}\right] \Big/ d^0_{(111)} \quad (1)$$

where $d^0_{(111)}$ is the nominal bulk (1 1 1) interplanar distance in the respective bulk phase at the given temperature. The range of the 2theta values in the used transmission geometry is<30°, which implies that all the diffracting planes lie in the bisecting line (i.e. in 15°) with respect to the surface normal. Thus all the reflections measured are almost perpendicular to the surface and the strain derived by the peak deviation with bulk is “almost” an in-plane strain assuming a uniform volumetric strain. For this reason, the word average strain is more representative of the quantity measured being not exactly an in plane component. Moreover, during the oxidation and reduction transformations, the formed oxide or metal nanostructures are entirely polycrystalline with no texture (as compared to epitaxial and highly-textured thin films) so the strain calculated for the $d_{(1\,1\,1)}$ can be considered as representative of the average strain in the sample. For the strain calculation, the $d^0_{(111)}$ reference values at room temperature were extrapolated to the targeted temperature using the reported thermal expansion coefficients for each corresponding bulk phases [31,32]. To trace the phase evolutions of the Cu, Cu_2O and CuO phases, the integrated peak areas of the most intense peaks for each phase were analyzed as a function of time (note: the integrated peak area scales with the scattering volume of the corresponding phase). The effective layer thickness of the single-phase Cu_2O or CuO films after full oxidation of the Cu film (for an initial metallic

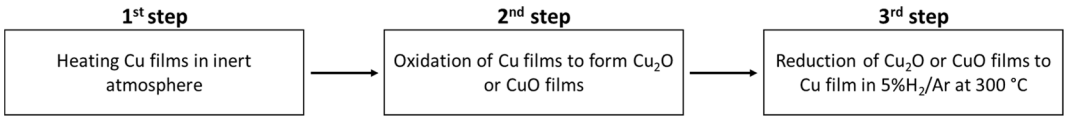

Fig. 1. Schematic illustration of the successive heating, oxidation and reduction steps performed during the in-situ synchrotron experiment.

layer thicknesses of either 50, 150 or 300 nm) was calculated based on the Pilling-Bedworth ratios (PBR) for each oxide. This resulted in thicknesses for the single-phase Cu_2O: ~80 nm, ~250 nm and ~ 500 nm and for the CuO: of ~ 90 nm, ~270 nm and ~ 530 nm for an initial Cu film thickness of 50 nm, 150 nm and 300 nm, respectively.

3. Results and discussion

3.1. Oxidation of Cu metal films into single-phase Cu_2O and CuO films

Oxidation of the 300-nm-thick Cu films was performed in synthetic air (20 vol%–O_2/Ar) at 300 °C and 400 °C to obtain single phase of Cu_2O and CuO, respectively, while conducting XRD analysis in transmission mode to capture the oxide phase evolution. False color XRD maps for the 2theta range of interest were constructed by stacking the successively recorded diffractograms in Fig. 2a and 2c. The evolution of the Cu → Cu_2O or Cu → Cu_2O → CuO phase constitution by time is visualized by plotting the normalized integrated areas of the peaks as representative for each phase as a function of the oxidation time in Fig. 2b and 2d.

As follows from Fig. 2a, oxidation of the Cu film at 300 °C results the single phase formation of Cu_2O. The corresponding Cu_2O growth curve shown in the inset of Fig. 2b (derived from the normalized integrated peak area of the evolving most intense Cu_2O peak) evidences the linear oxidation of Cu to-Cu_2O with a rate constant of $k = 1.1 \times 10^{-7}$ cm/s. It has to be mentioned that the magnetron-sputtered Cu films exhibit a strong (1 1 1) out-of-plane texture [33]. For such textured films, only a limited number of reflections are probed in the adopted transmission geometry. Therefore, the Cu(1 1 1) reflection is relatively weak. Notably, the plateau in the diffracted intensity reached after ~ 700 s of oxidation reflects full consumption of the Cu thin film. The linear oxidation rate of the 300 nm Cu film at 300 °C derived by in-situ XRD is in good agreement with the corresponding oxidation rates in a previous study at various oxygen partial pressures for film thicknesses between 20 and 150 nm by in-situ resistance measurements [33].

The temperature dependence of the Cu_2O phase formation kinetics for the 300 nm Cu films in the temperature range of 275 to 350 °C is shown in the supplementary Fig S1. As expected, the linear growth rate of the Cu_2O phase increases with increasing temperature. The corresponding activation energy, E_a is 0.5 ± 0.1 eV (see inset of Fig. S1) in excellent agreement with corresponding values obtained by in-situ

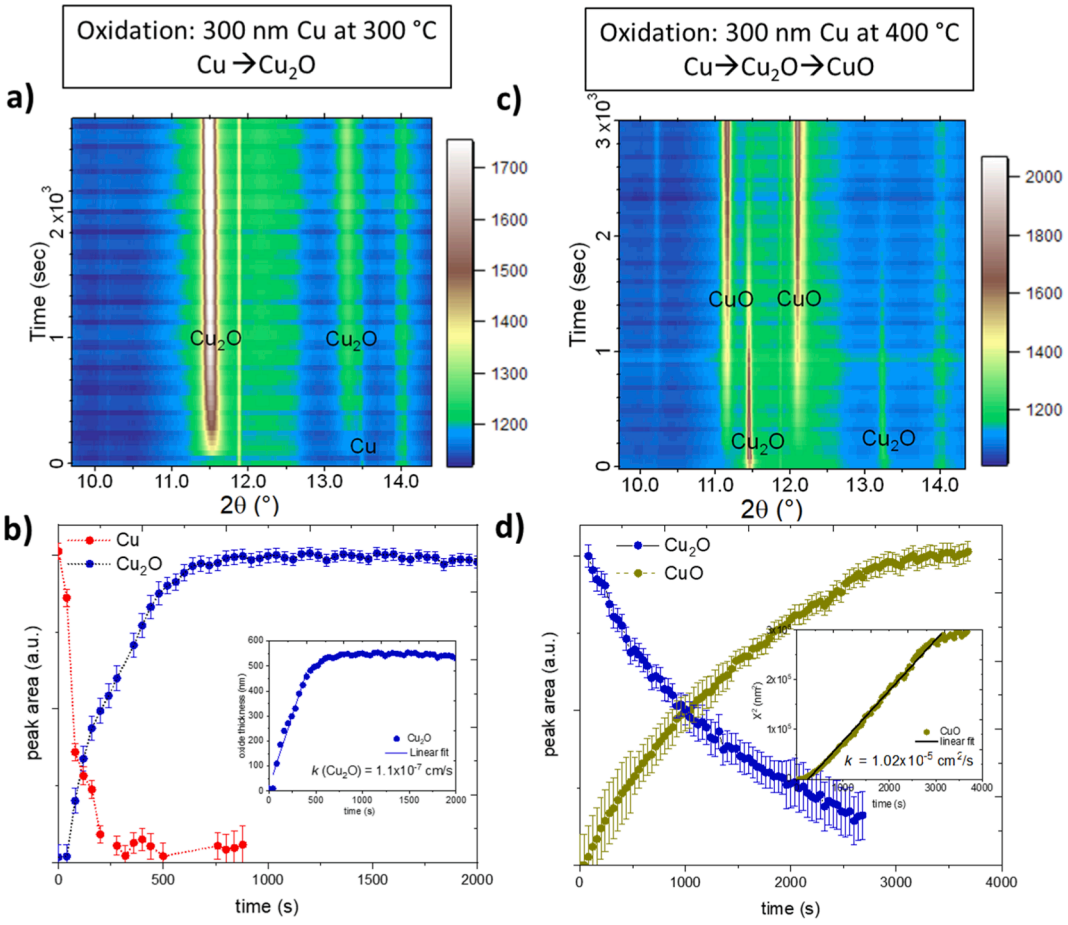

Fig. 2. In-situ time-resolved XRD analysis of the thermal oxidation of 300-nm-thick Cu films to single phase of Cu_2O and CuO in 20 vol%–O_2 / Ar. (**a,c**) False color in-situ X-ray diffraction (λ = 0.4921 Å) maps for the oxidation at 300 °C and 400 °C, respectively. (**b,d**) Normalized integrated area of the respective peaks as a function of the oxidation time at 300 °C and 400 °C, respectively. The insets in (b) and (d) evidence the linear oxidation rate for the Cu → Cu_2O phase transformation at 300 °C and the diffusion-controlled oxidation rate for the Cu_2O → CuO phase transformation at 400 °C, respectively.

resistance measurements for 20, 50 and 150 nm thick Cu films in previous studies [33]. As postulated in Ref. [33], the derived value of $E_a = 0.5 \pm 0.1$ eV represents the effective energy barrier for dissociative chemisorption of O_2(g) molecules on Cu_2O. Notably, thin film oxidation of other transition metals, such as Cr, Al, Ti, Co, and Ni, under similar conditions are not associated with linear oxidation kinetics (indicative for surface-limited growth). Instead the parabolic (diffusion-controlled) growth rate is observed for other transition metals, which indicates that the diffusion of the reactants through the thickening oxide layer (i.e. O anions and/or metal cations and their respective vacancies) is rate-limiting.

The evolutions of the average grain size and the average strain of the Cu and Cu_2O phases during oxidation of the 300-nm-thick Cu film at 300 °C are presented in the supplementary material Fig. S2b and S2c, respectively. It follows that the initial columnar grain length of Cu steadily decreases with time due to the conversion of the Cu film into Cu_2O. As expected in parallel and corresponding to the Cu grain shrinking, the Cu_2O grain size increases, reaching an average grain size of about 32 nm at the end of the oxidation step. The developing Cu_2O phase has an initial compressive strain as large as −0.5% (Fig. 1Sc), which gradually relaxes towards zero at the end of the oxidation. The Pilling-Bedworth ratios (PBR) of Cu_2O and CuO is around 1.7 and 1.8, respectively [34] which are much larger than unity, explaining the initial compressive strain in the Cu_2O growth [35]. Outward diffusion of Cu cations from the Cu/Cu_2O interface to the Cu_2O surface are balanced by an inward flux of cation vacancies, which both occur at a much faster rate than the inward diffusion of oxygen anions. This results in the development of Kirkendall voids [36] at the inwardly migrating Cu/Cu_2O interface during oxidation (and ending at the substrate interface when the process is completed), as evidenced by cross-sectional SEM analysis of partially oxidized Cu films in the present study (see Fig. S3). In parallel to Kirkendall voiding during oxidation, the relaxation of film stresses during the Cu → Cu_2O transformation occurs via Cu vacancy formation. The initial compressive strain in the Cu_2O phase has fully relaxed after complete oxidation of the Cu metal film (Fig. 2c) and the Kirkendall voids are residing at the Cu_2O-film/Al_2O_3-substrate interface. A detailed discussion is given in Section 3.2 for Fig. 5.

First detectable traces of the CuO phase appear after ~ 1000 s of oxidation at 300 °C (not visible in the color plot in Fig. 2a), only after the initial Cu film is fully transformed into Cu_2O. This indicates that although some CuO has nucleated on the outer Cu_2O surface after prolonged oxidation at 300 °C, the nucleated CuO phase does not grow at the expense of the Cu_2O phase. As evidenced by marker experiments on the oxidation of Cu_2O films at higher temperatures (700 – 1000 °C), the Cu_2O → CuO oxidation is realized by the outward diffusion of Cu cations via a cation vacancy transport mechanism (and not by the diffusion of oxygen anions and/or their vacancies) [37]. As discussed in detail below, the diffusion of Cu in CuO is much slower than of Cu in Cu_2O as shown in Ref. [37]. Consequently, at 300 °C, the thermally activated diffusion of Cu in CuO under influence of the chemical potential gradient across the oxide film is still too slow to transform the initially formed Cu_2O layer into CuO within a reasonable time frame.

As evidenced in the false color in-situ X-ray diffraction map for the oxidation of a 300 nm thick Cu film at 400 °C (Fig. 2*c*), a complete transformation of the initial 300-nm-thick Cu film into CuO can be achieved within 1 h of oxidation at 400 °C. This is in excellent agreement with a literature study for the thermally-activated Cu_2O to CuO phase transformation in the temperature range of 350 – 450 °C where it is also reported that the Cu_2O to CuO transformation temperature strongly depends on the film microstructure, in particular on the Cu_2O grain size [38]. Apparently, the initial stage of oxidation of Cu into Cu_2O at 400 °C occurs at such a high rate that only the oxidation stage of Cu_2O into CuO can be captured using the employed time step of the XRD measurement of 40 s (see Fig. 2*c and d*). In order to be able to capture the Cu to Cu_2O oxidation at 400 °C, the XRD measurement time step should be further decreased (at the expense of the measurement statistics).

The respective CuO growth curve in Fig. 2*d* obeys a parabolic growth law, which indicates that the Cu_2O → CuO transformation rate is diffusion controlled, in accordance with Ref. [37]. The corresponding parabolic growth rate is found to be $k_{p\ (CuO)} = 1.02 \times 10^{-5}$ cm^2/s at 400 °C in this study, see the inset in Fig. 2d. On the contrary, the initial oxidation stage of Cu thin films, as associated with the conversion of Cu into Cu_2O, follows a linear growth rate, indicative of a surface-controlled reaction under the given condition (see Fig. 2*b* and the inset). This change in the oxide growth mechanism can be explained by the relative sluggish diffusion of Cu in the CuO lattice and/or its grain boundaries as compared to the much faster diffusion of Cu in the Cu_2O lattice and/or its grain boundaries [27,39,40]. It should be noted that, as in most binary oxides, Cu cation diffusion coefficients in Cu_2O and CuO are much faster than the respective oxygen anion diffusion coefficients (up to 5 orders of magnitude at 1000 °C) [37,41,42]. For example, the Cu self-diffusion coefficient in bulk CuO at 1000 °C equals ~ 1×10^{-16} cm^2/s [37], which is much smaller than the self-diffusion of Cu in bulk Cu_2O at 1000 °C of ~ 2×10^{-11} cm^2/s [43]. Consequently, only at oxidation temperatures above 300 °C, the Cu_2O-to-CuO transformation becomes thermally activated at a reasonable rate. As reflected in Fig. S2e, the grain size evolutions of Cu_2O and CuO during oxidation at 400 °C seems to develop independently. The Cu_2O grain size, as established after complete oxidation of Cu, is around 43 nm, while the CuO grain size is about half this size (22 nm at the beginning of the transformation): See Fig. S2d. This indicates that the Cu_2O grains are not simultaneously transformed into CuO. Probably, the surface-adjacent Cu_2O grains are transformed first, possibly nucleating multiple CuO domains within a single Cu_2O grain. Subsequently, Cu_2O grains below the formed CuO grains are transformed in a layer-by-layer fashion. Due to the limited O and Cu mobilities in CuO as compared to Cu_2O (see above), the CuO phase develops a smaller grain size by grain growth (at constant temperature). Compressive strain occurs during CuO formation line with the slightly smaller strain-free $d_{(111)}$ spacing of CuO (2.315 Å) as compared to Cu_2O (2.455 Å; only a slight tensile strain resides in Cu_2O): See Fig. S2f.

The above findings on the oxidation kinetics of thin Cu films in synthetic air by synchrotron XRD are in excellent agreement with our previous study on the effect of the oxygen partial pressure on the oxidation kinetics of Cu thin films by in-situ resistance measurements [33]. Cu thin-film oxidation starts with the fast formation of Cu_2O; only after full oxidation of the Cu thin film, the CuO phase starts to grow; a co-existence of Cu, Cu_2O and CuO phases during the oxidation process was not observed [33]. Much thicker Cu films, comparable to bulk-like Cu metal specimens, are required to observe the co-existence of Cu, Cu_2O and CuO under the applied conditions, e.g., 400 °C in air [31]. On the basis of the obtained findings on the oxidation of the Cu thin films, single-phase oxide films of either CuO or Cu_2O were produced for studying the corresponding reduction kinetics in 5 vol%–H_2/Ar at 300 °C by in-situ time-resolved XRD.

3.2. *Reduction of a single-phase CuO film*

A ~ 530 nm thick CuO film was produced by oxidation of a 300 nm thick Cu film for 1 h at 400 °C in synthetic air (Fig. 2c). The single-phase CuO film was efficiently reduced in 5 vol%–H_2/Ar at 300 °C. The corresponding false color XRD map is shown in Fig. 3a. The integrated areas of the representative diffraction peaks of Cu, Cu_2O and CuO are plotted as a function of the reduction time in Fig. 3b. The curves are representative for the evolution of the volume fractions of the corresponding phases during the reduction process.

As reflected in Fig. 3a, the phase transformation sequence during reduction at 300 °C can be well-monitored by in-situ time-resolved XRD and proceeds according to CuO → CuO + Cu_2O → CuO + Cu_2O + Cu → Cu_2O + Cu → Cu. Strikingly, a three phase coexistence of Cu, Cu_2O and CuO is observed during reduction, but not during oxidation. Notably, the onset of the reduction process is only detected after a relatively long

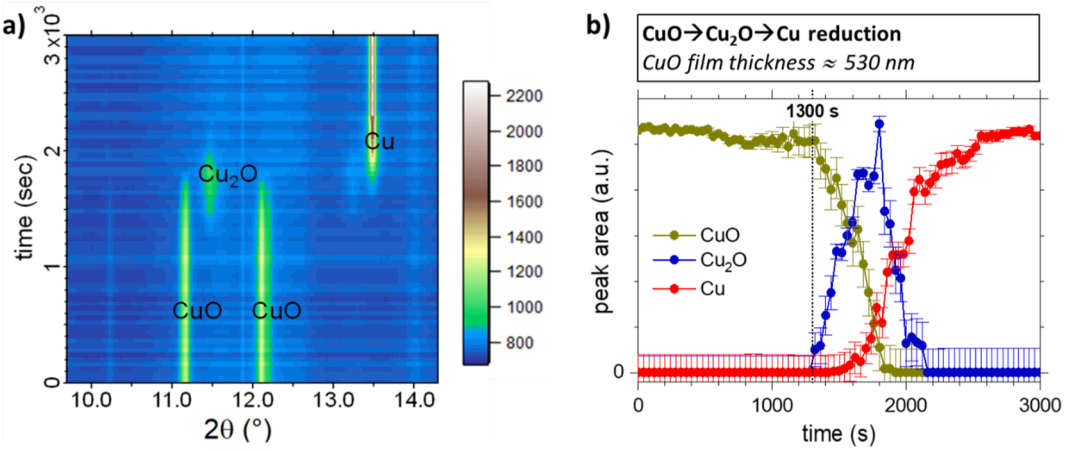

Fig. 3. Reduction of a single-phase CuO film at 300 °C in 5 vol%–H_2/Ar atmosphere. The CuO film was produced by oxidation of a 300 nm thick Cu film for 1 h at 400 °C in synthetic air and has an equivalent thickness of about 530 nm. (a) False color in-situ X-ray diffraction map recorded during the reduction. (b) Normalized integrated area of representative diffraction peaks of CuO, Cu_2O and Cu in (a), evidencing the co-existence of Cu, Cu_2O and CuO prior to full reduction to Cu.

incubation time of about 1300 s. The formation of metallic Cu by reduction of Cu_2O only prevails once a significant fraction of CuO has transformed into Cu_2O. The corresponding reduction reactions are:

$$2CuO(s) + H_2(g) \rightarrow Cu_2O(s) + H_2O(g) \quad (2)$$

$$Cu_2O(s) + H_2(g) \rightarrow 2Cu(s) + H_2O(g) \quad (3)$$

The initial reduction of CuO by H_2 according to Eq. (2) requires adsorption and dissociation of H_2. The incubation time for the reduction of CuO, as evidenced in Fig. 3, has been attributed to the time required for the initial generation of a high concentration of oxygen vacancies at the oxide surface, which catalyze the adsorption and dissociation of H_2 molecules [1,2,18]. As predicted by DFT calculations [16-18], the dissociative adsorption of H_2 gas molecules on the pristine CuO(1 1 1) surface leads to spontaneous formation of a water molecule, as accompanied by the reduction of two Cu^{2+} cations to Cu^+ and the creation of an oxygen vacancy at the surface (upon desorption of the H_2O molecule into the gas phase). The reactivity of the CuO(1 1 1) surface increases with the generation of oxygen vacancies by this spontaneous H_2O formation mechanism. As shown in Refs. [16-18], the continuous generation of oxygen vacancies at the CuO surface eventually leads to the coexistence of Cu^+ and Cu^0 at the surface. The formed oxygen vacancies migrate into the subsurface and self-order to form a partially reduced CuO superlattice structure, from which the Cu_2O phase can nucleate [18]. The incubation time for the CuO → Cu_2O reduction process can thus be substantially shortened for initially highly defective CuO surfaces (as produced by e.g. vacuum annealing or cyclic oxidation and reduction), as well as with increasing temperature and increasing hydrogen partial pressure [1,2]. On the contrary, the incubation time for CuO reduction in H_2 is increased for oxygen pre-covered CuO(1 1 1) surfaces, since they will first be hydroxylated upon exposure to H_2 (by forming OH surface species, instead of O vacancies) [17,18]. Analogously, exposure to water vapor also strongly inhibits the subsequent reaction between hydrogen and the Cu-oxide surface [20]. Accordingly, the relative long incubation time of about 1300 s, as observed for the reduction of a ~ 530 nm thick single-phase CuO film in the present study (Fig. 3), can be attributed to an initial hydroxylation of the O-terminated CuO film surface upon switching from O_2 to H_2 exposure. This process delays the formation of O vacancies by H_2O formation and desorption, which in turn delays the nucleation of Cu_2O domains [18,44].

Fig. 3 clearly evidences a co-existence of all three phases Cu, Cu_2O and CuO during the reduction process. The intermediate formation of Cu_4O_3 (CuO → Cu_4O_3 → Cu_2O → Cu) during reduction, as reported in e.g. Ref. [22], was not observed in this study. As argued in Ref. [2], the formation of Cu_4O_3 as a suboxide or an intermediate product during the reduction of CuO is kinetically obstructed due to the large structural mismatch between CuO and Cu_3O_4. Previous theoretical [16,18,45] and experimental studies [2] on the reduction of Cu-oxide in hydrogen conclude that the Cu_2O → Cu process is slower than the CuO → Cu reduction process. Nonetheless, previous in-situ diffraction studies on the reduction of submicron-sized CuO powders in a 5 vol% H_2/He gas mixture in the temperature range between 150 and 300 °C did not detect the intermediate formation of Cu_2O (nor Cu_4O_3) [1,2]. Instead a direct reduction of CuO to Cu according to

$$CuO(s) + H_2(g) \rightarrow Cu(s) + H_2O(g) \quad (4)$$

was reported [1,2]. These previous in-situ diffraction studies were performed with a considerable larger measurement time step of up to 3 min on CuO powders with unspecified particle size and shape distributions. The lower time resolution in combination with a nonuniform particle size distribution, a high density of catalytic step edges for H_2 dissociation (characteristic for facetted particles) [18,21,46], as well as a relatively high specific surface area, may have obscured the intermediate formation of Cu_2O from these previous CuO powder reduction studies. This assertion is supported by the fact that, in these previous studies, intermediate formation of Cu_2O upon reduction could be detected at a relatively low H_2 flow rate [1,2]. Dense, single-phase CuO and Cu_2O films, as used in the present study, are clearly better suited for studying the reduction kinetics by synchrotron X-ray diffraction.

3.3. *Reduction of a single-phase Cu_2O film*

During the Cu oxidation at 300 °C only the single phase Cu_2O is formed. The co-existence of all three phases Cu, Cu_2O and CuO was indeed observed only during reduction at 300 °C (compare Fig. 2a,b and 3a,b). As discussed in Section 3.1, the growth of CuO cannot be kinetically activated in a reasonable rate to detect during oxidation at 300 °C and, consequently, a three-phase coexistence is not observed. As presented in Fig. 2a,b, the Cu → Cu_2O transformation during oxidation of 300-nm-thick Cu films at 300 °C starts very fast (at ~ 0 s) and it is completed within about 700 s. The reverse Cu_2O → Cu transformation during reduction at 300 °C (see Fig. 4a) is significantly slower as compared to the oxidation at the same temperature, as it starts after ~ 680 s and completed within about 1800 s. To compare the rates of the Cu_2O → Cu and Cu_2O → Cu transformations in more detail, the Cu_2O → Cu reduction rate at 300 °C was determined by reduction of a single-phase Cu_2O film, as prepared by thermal oxidation of a 300 nm Cu film at 275 °C (Fig. S4a). This latter temperature for Cu → Cu_2O oxidation was intentionally chosen below 300 °C in order to avoid the

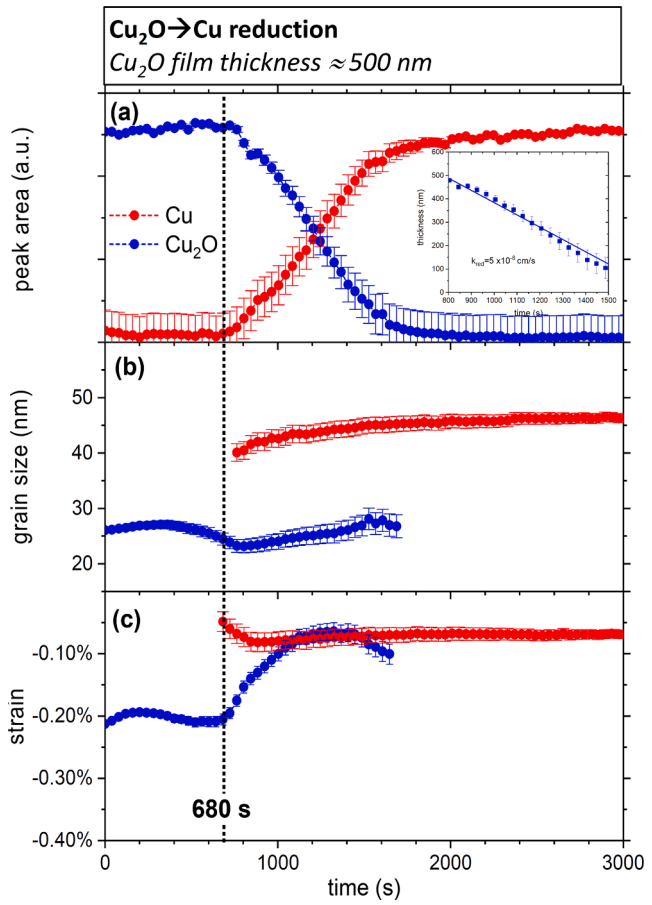

Fig. 4. Reduction of a single-phase Cu_2O film at 300 °C in 5 vol%–H_2/Ar, as monitored by in-situ time-resolved XRD. The ~ 500 nm thick Cu_2O film was produced by thermal oxidation of a 300 nm thick Cu film at 275 °C. (**a**) Integrated Cu_2O and Cu peak areas as function of the reduction time. In the inset, the linear reduction rate is extracted. (**b**) Average Cu_2O and Cu grain size as function of the reduction time (as derived using the Scherrer formula). (**c**) Average strain in the evolving Cu_2O and Cu phases (with respect to the unstrained bulk phase) as a function of the reduction time. The dotted line indicates the incubation time during which the formation of metallic Cu domains is not yet detected. False color in-situ X-ray diffraction map for Cu2O reduction is given in Fig. S4c in supplementary material.

formation of CuO at the surface and to end up with a single Cu_2O phase. The respective time evolutions of the normalized integrated areas of the selected Cu_2O and Cu diffraction peaks are shown in Fig. 4a, see the false color XRD maps in Fig. S4. The average grain sizes and strain levels in Cu_2O and Cu are plotted as function of the reduction time in Fig. 4b and 4c, respectively.

It follows that the $Cu_2O \rightarrow Cu$ reduction rate, $\underline{k}_{red} = 5 \times 10^{-8}$ cm/s at 300 °C in 5 vol% H_2 (see inset in Fig. 4a, incubation time is not considered) is indeed lower than the respective $Cu \rightarrow Cu_2O$ oxidation rate, $\underline{k}_{ox} = 1.1 \times 10^{-7}$ cm/s at 300 °C in 20 vol% O_2(g) (Fig. 2) for the identical samples. This implies that the requirements on the time resolution of the XRD measurements for capturing the complete phase transformation sequence are more severe for the Cu oxidation experiments. As seen in Section 3.1, after the oxidation of Cu to Cu_2O, complete strain relaxation occurs in the formed oxide, accompanied by Kirkendall void formation at the substrate interface. During the reduction, the Cu_2O film has an average compressive strain of about −0.2%, which should originate from the interaction of the relaxed Cu_2O film with the reducing H_2/Ar atmosphere. During the H_2 exposure, intersecting grain boundaries and porosity at the Cu_2O film surface will act as short-circuit diffusion paths and trapping sites for hydrogen. The diffusion of hydrogen along intergranular regions can induce a compressive stress, analogously to the generation of compressive stresses by inward diffusion of adatoms along grain boundaries during film growth [47,48]. In addition, the accumulation of O vacancies at intergranular Cu_2O regions may generate compressive stresses in the Cu_2O phase, as explained in the following. As discussed in Section. 3.2, O vacancies accumulate at the rim of Cu_2O grains which interact with H_2. This will lead to a partial distortion of the crystal lattice at the periphery of the Cu_2O grains, generating tensile strain contributions, which will be counteracted by compressive strain contributions in the interior of the grains. Although the validity of such O-vacancy induced stress generation is debatable this mechanism would rationalize not only the development of an overall compressive strain in the Cu_2O phase during the incubation time, but also the accompanied apparent gradual decrease of the average grain size (see Fig. 4b) as seen in Ref [18].

As discussed in Section 3.1, the PBRs for Cu_2O and CuO are much larger than unity and, consequently, reduction of Cu_2O (or CuO) to Cu metal induces a volume shrinkage. Initially, the nucleated Cu domains will still be largely coherent to the parent Cu_2O grains and the Cu_2O phase has a much higher compressive strain (≈ –0.2%) than the Cu phase (≈ −0.05%). The accumulation of volumetric strains during the $Cu_2O \rightarrow Cu$ transformation step (i.e. during further growth of Cu metal grains) results in an open grain boundary structure and may eventually induce intergranular cracking, as observed in Refs. [49,50]. Intergranularity at the grain boundary enables fast relaxation of accumulated film stresses, as indeed evidenced in Fig. 6c. These open grain boundaries act as short-circuit paths for fast inward diffusion of molecular hydrogen, thereby increasing the effective surface area for dissociative adsorption of H_2. Except for an initial small increase during the post-nucleation stage, the strain level in the Cu phase remains relatively low and practically constant until the $Cu_2O \rightarrow Cu$ transformation has completed. The Cu grain size gradually increases by grain growth.

SEM micrographs of the as-deposited 300-nm-thick Cu film, as well as of the reduced Cu at 300 °C in 5 vol%–H_2/Ar, are shown in Fig. 5 (a-c). It follows that the as-prepared dense Cu metal film (Fig. 5a) is effectively transformed into a highly porous Cu scaffold (Fig. 5b and 5c) by initial oxidation and subsequent reduction. It is worthy to mention that the average size and shape of the final Cu scaffold depends on the original microstructure of the formed oxide phase (either Cu_2O or CuO film) and, in particular, its grain size, as shown in Fig. 6. The extended voids along the original Cu/Al_2O_3 interface, as observed in Fig. 5b, primarily originate from Kirkendall voiding during the oxidation step.

3.4. *Effect of the CuO film thickness on the reduction kinetics*

As follows from the above discussion, the $CuO \rightarrow Cu_2O$ and $Cu_2O \rightarrow Cu$ transformations run in parallel, as primarily governed by the temperature, the film thickness (as well as the chemical activity of hydrogen which is not the scope of this work). This implies that, depending on the individual transformation rates, the phase transformation sequence may be partially obscured from the XRD analysis, depending on external experimental variables such as the temperature, hydrogen partial pressure, defect density, measurement time step, as well as the sample's dimensions and surface morphology. The effect of the CuO film thickness on the phase evolution during reduction at 300 °C was investigated by reducing the initial CuO film thickness from ~ 530 nm to ~ 90 nm (corresponding to initial Cu film thicknesses of 300 and 50 nm, respectively). The measured phase evolution during reduction of the thin CuO film is shown in Fig. 6a and can be compared to that of the thick CuO film in Fig. 6b. The corresponding average grain sizes and strain levels are plotted as a function of the reduction time in Fig. 6(c,d) and Fig. 6(d,f), respectively.

Strikingly, a threephase co-existence during reduction is not observed for the thinner CuO film; reduction of Cu_2O to Cu metal only commences after full reduction of the initial CuO layer into Cu_2O. Theoretical [16,18,45] and experimental studies [2] on the reduction of

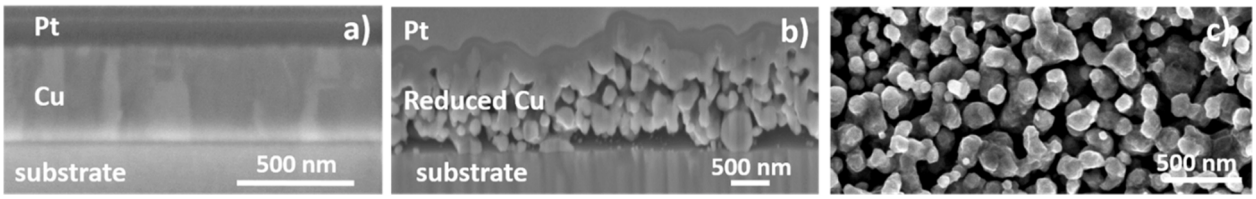

Fig. 5. SEM micrographs of a 300-nm-thick Cu film in the as-deposited state, and after -reduction of the oxidized Cu_2O film. (**a**) Cross section of the as-deposited Cu film. the initial Cu film was oxidized at 275 °C to form a single-phase Cu_2O film and subsequently fully reduced at 300 °C in 5 vol%–H_2/Ar. (**b**) Cross-sectional and (**c**) planar SEM micrograph of the nanoporous Cu scaffold obtained by reduction.

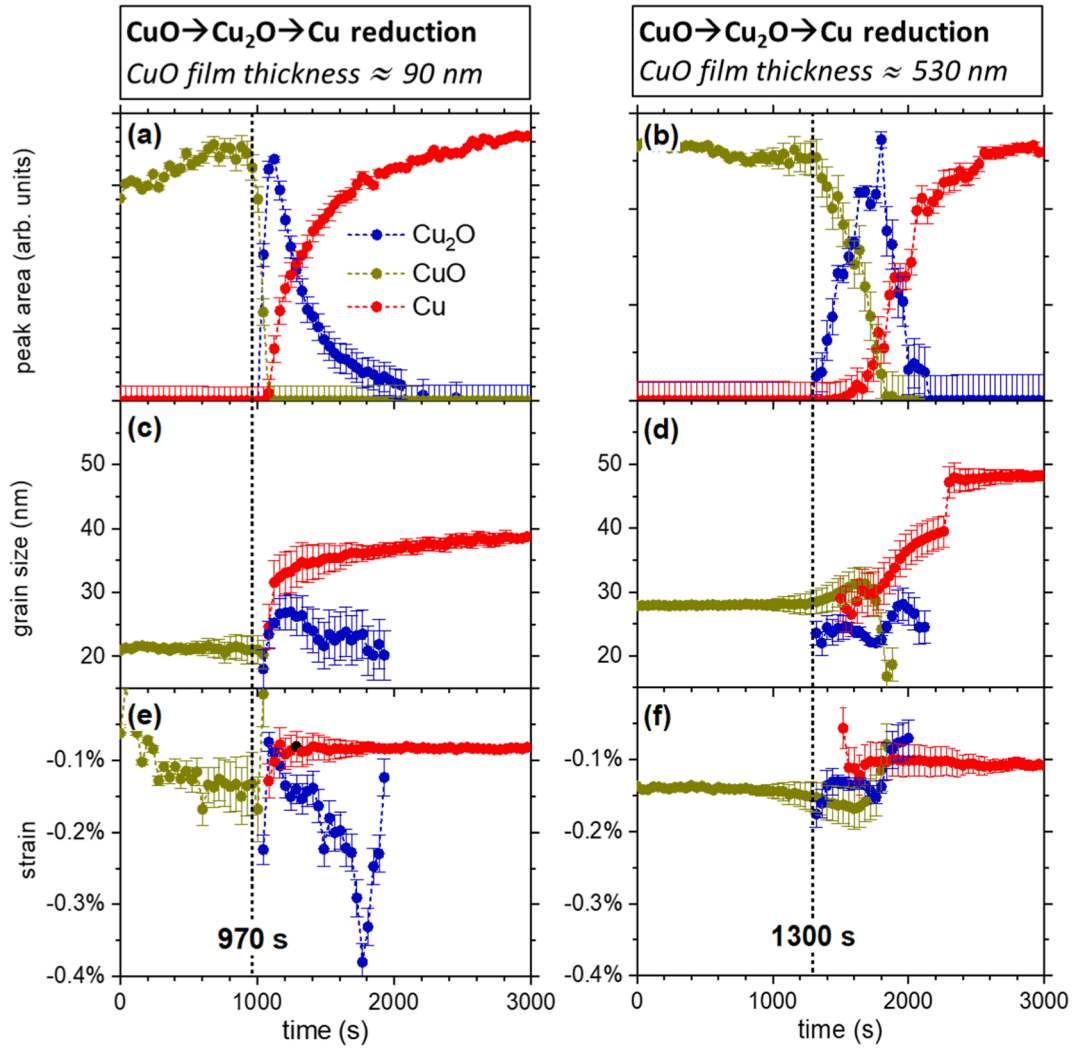

Fig. 6. Reduction of single-phase CuO films with thicknesses of 90 nm and 530 nm at 300 °C in 5 vol%–H_2/Ar, as monitored by in-situ time-resolved XRD. (**a,b**) Integrated CuO, Cu_2O and/or Cu peak areas as function of the reduction time. (**c,d**) Average CuO, Cu_2O and/or Cu grain size as function of the reduction time. (**e,f**) Average strain in the evolving CuO, Cu_2O and/or Cu phases as function of the reduction time. The ~ 90 nm thick CuO film is produced by oxidation of a 50 nm thick Cu film at 300 °C. The ~ 530 nm thick CuO film is produced by oxidation of a 300 nm thick Cu film at 400 °C (identical data set to the data set in Fig. 3a,b).

Cu-oxide in hydrogen have concluded that the CuO → Cu_2O (i.e. Cu^{2+} →Cu^{+}) reduction process is energetically more favorable than the Cu_2O → Cu (i.e. Cu^{+} →Cu^{0}) process under the same hydrogen partial pressure and temperature. Moreover, a supersaturation of under-coordinated Cu metal atoms at the Cu_2O surface is required [18] to trigger the nucleation of metallic Cu domains [27]. Consequently, for very thin CuO films, the fast CuO → Cu_2O transformation may have been completed prior to the detection of the Cu phase by XRD.

As presented in Fig. 6, the incubation time for the onset of the CuO → Cu_2O reduction is reduced from 1300 s to 970 s by decreasing the initial CuO film thickness from 530 nm to 90 nm As discussed in Section 3.2, the incubation time is attributed to the "activation" of the CuO surface for dissociative adsorption of H_2, which should be independent of the CuO thickness. However, the thinner CuO film is produced at a lower oxidation temperature (300 °C) and therefore has a smaller average grain size by grain growth (~ 20 nm) as compared to the thicker CuO film (as produced at an oxidation temperature of 400 °C, resulting in a grain size of ~ 30 nm). Intersecting grain boundaries and porosity at the CuO film surface will act as short-circuit diffusion paths and trapping sites of hydrogen, thus allowing inward penetration of the reduction

front. The higher grain boundary density of the thinner CuO film at the surface will thus results in a substantial shorter incubation time. Hence, the competition between the CuO → Cu_2O and Cu_2O → Cu reduction rates crucially depends on the initial grain size at the surface of the parent CuO/Cu_2O film, which has been disregarded up to date.

Moreover, as follows from kinetic considerations, the hydrogen concentration across the CuO film will be much steeper for smaller CuO film thicknesses, which further promotes the generation of oxygen vacancies and thereby increase the reduction rate. Indeed the CuO → Cu_2O reduction rate is much higher for the thin CuO film (90 nm vs 530 nm, compare Fig. 6a and 6b).

Strikingly, although the initial grain sizes of the thin and thick CuO film are different (20 nm vs. 30 nm), the final Cu_2O grain size evolution during the CuO → Cu_2O reduction stage is similar for both films (deviating between 20 and 28 nm), independently of the initial thickness and of the presence of the three-phase coexistence. This suggests that the formation of the Cu_2O grains occurs rather heterogeneously at the peripheries of the H_2 exposed CuO grains and it is governed by the reduction temperature, in accordance with Refs. [28,51].

As discussed above, the CuO → Cu_2O and Cu_2O → Cu phase transformations are detected sequentially for the reduction of the thin CuO film (90 nm), whereas a three-phase coexistence is observed only for the reduction of the thicker CuO film (530 nm). During the Cu_2O → Cu transition, the thin CuO film exhibits a gradual increase of the Cu grain size during the reduction process (Fig. 6c), indicative for Cu grain growth. The thick CuO film also shows a gradual increase of the Cu grain size by grain growth, which is followed by a non-monotonic sudden increase of the Cu grain size at the end of the reduction process (Fig. 6d) by grain coalescence (as triggered by upon complete disappearance of all oxide phases).

The general trend in the strain evolution of the developing Cu_2O phase is independent of the phase coexistence during reduction, see Fig. 6e and 6f. During the initial stage of Cu grain formation and growth, the Cu_2O phase develops a higher compressive strain than the Cu phase (see Section 3.3), which relaxes by pore formation at the final stage of the reduction process. Although the strain curves are similar in shape, the thinner Cu_2O film can sustain much higher compressive strain levels (of up to −0.4%) prior to relaxation, as is also evidenced in Fig. 6e.

SEM analysis of a nanoporous Cu film obtained by reduction of a single-phase CuO film at 300 °C is shown in Fig. 7a. It follows that the nanoporous Cu scaffold obtained by reduction of the single-phase CuO film has smaller grains and pores (resulting in a different open porosity) than the Cu scaffold obtained by reduction of the single-phase Cu_2O film: compare Fig. 7a and 5c. The Cu grain size after reduction depends on the grain size of the Cu_2O phase, which is indeed slightly smaller for the reduction of the CuO film (compare Fig. 6d with Fig. 4b, ~20 nm vs 28 nm at the beginning of the process). As shown in Fig. 7b, the porous Cu scaffold obtained after reduction can be reoxidized to obtain single-phase CuO (or Cu_2O) scaffolds with a very high specific surface area. Such porous CuO and Cu_2O scaffolds can be envisaged for a wealth of applications in the field of e.g. catalysis, batteries, water treatment and biomedical applications.

4. Conclusions

Single-phase Cu_2O and CuO thin films of various thicknesses were prepared by thermal oxidation of magnetron-sputtered Cu films in synthetic air, while monitoring the phase transformation sequence by in-situ time-resolved XRD. The Cu_2O → CuO phase transformation follows a diffusion-controlled growth law, whereas the Cu → Cu_2O oxidation kinetics obey a linear rate law, characteristic for surface-limited growth. The large difference in molar volume between Cu and Cu_2O, leads to the generation of compressive growth strains during oxidation, which are relaxed by the formation of Cu vacancies and associated Kirkendall voids at the inwardly migrating Cu/Cu_2O interface.

Single-phase Cu_2O and CuO thin films of variable thickness were reduced in 5 vol% H_2/Ar at 300 °C. For 50-nm-thick CuO films with an average grain size of ~ 20 nm, the formation of Cu metal is only detected after complete reduction of CuO to Cu_2O. On the contrary, for 300-nm-thick Cu films with an average grain size of ~ 30 nm, Cu metal is already detected before the complete reduction of CuO to Cu_2O phase, resulting in a three-phase coexistence. Intersecting grain boundaries and porosity at the Cu_2O film surface will act as short-circuit diffusion paths and trapping sites of hydrogen. Consequently, the higher grain boundary density of the thinner Cu_2O films results in a shorter incubation time and faster reduction rates. As a result, the CuO → Cu_2O transformation step is completed within a much short time for the thinner CuO film with a smaller grain size. Hence, the evolution from CuO → Cu_2O and Cu_2O → Cu reduction rates crucially depends on the initial grain size of the parent CuO or Cu_2O film, as well as the initial CuO or Cu_2O film thickness.

The reduction of the CuO or Cu_2O films in H_2 was found to be preceded by an incubation time during which oxygen vacancies are accumulated in the oxide subsurface region by H_2O formation and desorption. Formation of the product phase (either Cu_2O or Cu) is triggered once a certain density of accumulated oxygen vacancies is reached at the periphery of the grains of the parent phase (either CuO or Cu_2O).

Highly porous Cu scaffolds can be obtained by reduction of single-phase Cu_2O and CuO films, as produced by controlled oxidation of a Cu metal film. The average size and shape of the final Cu scaffold depends on the grain size and the thickness of the initial Cu-oxide phases. The porous Cu scaffold can be reoxidized to obtain single-phase CuO or Cu_2O scaffolds with a very high specific surface area. With all these insights regarding the controlled oxidation of Cu films into oxide phases and now well understood reduction kinetics of CuO or Cu_2O phases, this

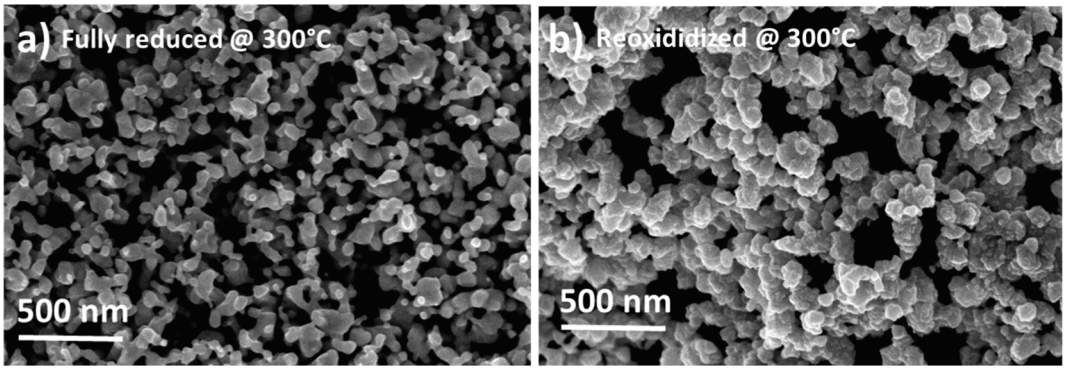

Fig. 7. (**a**) SEM micrograph of the surface of a nanoporous Cu film, as obtained after reduction of a single-phase CuO film at 300 °C in 5 vol% H_2/Ar. The initial dense CuO film was produced by oxidation of a 300-nm-thick Cu film at 400 °C. (**b**) SEM micrograph of the surface of a nanoporous CuO film, as obtained after reoxidation of a nanoporous Cu film (produced by oxidation of a 50-nm-thick Cu film oxidized at 200 °C and subsequent reduction at 300 °C in 5 vol% H_2/Ar.

work paves the way for tuning porosity in Cu thin films, highly relevant for specific catalysis applications.

CRediT authorship contribution statement

Yeliz Unutulmazsoy: Conceptualization, methodology, data acquisition, data analysis, writing and original draft preparation. **Claudia Cancellieri:** Conceptualization, data acquisition, data analysis, writing. **Luchan Lin:** Data acquisition, reviewing. **Lars P.H. Jeurgens:** Conceptualization, writing, reviewing, editing, funding.

Declaration of Competing Interest

The authors declare that they have no known competing financial interests or personal relationships that could have appeared to influence the work reported in this paper.

Acknowledgments

The authors thank Dr. Roland Hauert and Tobias Burgdorf for technical support with the preparation of the custom-designed microfurnace for the in-situ experiments at the synchrotron. Dr. Sebastian Siol is acknowledged for magnetron-sputter deposition of the Cu thin films. We are grateful for the on-site support by the beamline scientists, Dr. Nicola P. M. Casati and the technical staff, Michael Lange, of the MS-X04SA beamline at Swiss Light Source (SLS) in PSI Villigen. Yeliz Unutulmazsoy acknowledges funding from Innosuisse-Swiss Innovation Agency. Luchan Lin acknowledges funding from the European Union's Horizon 2020 research and innovation programme under the Marie Skłodowska-Curie grant agreement number 754364. The electron microscopy center and Michael Stiefel at the laboratory for transport at nanoscale interfaces at Empa are acknowledged for their support.

Appendix A. Supplementary data

Supplementary data to this article can be found online at https://doi.org/10.1016/j.apsusc.2022.152896.

References

[1] J.A. Rodriguez, J.Y. Kim, J.C. Hanson, M. Pérez, A.I. Frenkel, Reduction of CuO in H2: In Situ Time-Resolved XRD Studies, Catal. Lett. 85 (2003) 247–254, https://doi.org/10.1023/A:1022110200942.
[2] J.Y. Kim, J.A. Rodriguez, J.C. Hanson, A.I. Frenkel, P.L. Lee, Reduction of CuO and Cu2O with H2: H Embedding and Kinetic Effects in the Formation of Suboxides, J. Am. Chem. Soc. 125 (2003) 10684–10692, https://doi.org/10.1021/ja0301673.
[3] M.B. Gawande, A. Goswami, F.-X. Felpin, T. Asefa, X. Huang, R. Silva, X. Zou, R. Zboril, R.S. Varma, Cu and Cu-Based Nanoparticles: Synthesis and Applications in Catalysis, Chem. Rev. 116 (2016) 3722–3811, https://doi.org/10.1021/acs.chemrev.5b00482.
[4] R. Siavash Moakhar, S.M. Hosseini-Hosseinabad, S. Masudy-Panah, A. Seza, M. Jalali, H. Fallah-Arani, F. Dabir, S. Gholipour, Y. Abdi, M. Bagheri-Hariri, N. Riahi-Noori, Y.-F. Lim, A. Hagfeldt, M. Saliba, Photoelectrochemical Water-Splitting Using CuO-Based Electrodes for Hydrogen Production: A Review, Adv. Mater. 33 (33) (2021) 2007285, https://doi.org/10.1002/adma.v33.3310.1002/adma.202007285.
[5] A.C. Schilling, K. Groden, J.P. Simonovis, A. Hunt, R.T. Hannagan, V. Çınar, J.-S. McEwen, E.C.H. Sykes, I. Waluyo, Accelerated Cu2O Reduction by Single Pt Atoms at the Metal-Oxide Interface, ACS Catal. 10 (2020) 4215–4226, https://doi.org/10.1021/acscatal.9b05270.
[6] T. Yao, T. Matsuda, T. Sano, C. Morikawa, A. Ohbuchi, H. Yashiro, A. Hirose, In Situ Study of Reduction Process of CuO Paste and Its Effect on Bondability of Cu-to-Cu Joints, J. Electron. Mater. 47 (2018) 2193–2197, https://doi.org/10.1007/s11664-017-6049-9.
[7] K. Inami, T. Matsuda, R. Kawabata, T. Sano, A. Hirose, Lowering bonding temperature for silver sintering to silicon and silicon carbide using silver oxide decomposition, J. Mater. Sci.: Mater. Electron. 31 (19) (2020) 16511–16518, https://doi.org/10.1007/s10854-020-04205-w.
[8] D. Yamagiwa, T. Matsuda, H. Furusawa, K. Sato, H. Tatsumi, T. Sano, Y. Kashiba, A. Hirose, Pressureless sinter joining of bare Cu substrates under forming gas atmosphere by surface-oxidized submicron Cu particles, J. Mater. Sci.: Mater. Electron. 32 (14) (2021) 19031–19041, https://doi.org/10.1007/s10854-021-06418-z.
[9] A. Kuch, Investigations of the reduction and re-oxidation kinetics of iron(III) oxide scales formed in waters, Corros. Sci. 28 (3) (1988) 221–231, https://doi.org/10.1016/0010-938X(88)90106-0.
[10] C. Kenel, J.P.W. Sesseg, N.R. Geisendorfer, R.N. Shah, R. Spolenak, D.C. Dunand, 3D-printed tungsten sheet-gyroids via reduction and sintering of extruded WO3-nanopowder inks, Addit. Manuf. 36 (2020) 101613, https://doi.org/10.1016/j.addma.2020.101613.
[11] C. Kenel, N.R. Geisendorfer, R.N. Shah, D.C. Dunand, Hierarchically-porous metallic scaffolds via 3D extrusion and reduction of oxide particle inks with salt space-holders, Addit. Manuf. 37 (2021) 101637, https://doi.org/10.1016/j.addma.2020.101637.
[12] F. Klein, R. Pinedo, B.B. Berkes, J. Janek, P. Adelhelm, Kinetics and Degradation Processes of CuO as Conversion Electrode for Sodium-Ion Batteries: An Electrochemical Study Combined with Pressure Monitoring and DEMS, J. Phys. Chem. C 121 (2017) 8679–8691, https://doi.org/10.1021/acs.jpcc.6b11149.
[13] E.A. Souza, R. Landers, L.P. Cardoso, T.G.S. Cruz, M.H. Tabacniks, A. Gorenstein, Evaluation of copper oxide thin films as electrodes for microbatteries, J. Power Sources 155 (2) (2006) 358–363, https://doi.org/10.1016/j.jpowsour.2005.04.014.
[14] B. Laik, P. Poizot, J.-M. Tarascon, The Electrochemical Quartz Crystal Microbalance as a Means for Studying the Reactivity of Cu[sub 2]O toward Lithium, J. Electrochem. Soc. 149 (2002) A251, https://doi.org/10.1149/1.1445430.
[15] A. Rydosz, The Use of Copper Oxide Thin Films in Gas-Sensing Applications, Coatings 8 (2018) 425.
[16] Y. Maimaiti, M. Nolan, S.D. Elliott, Reduction mechanisms of the CuO(111) surface through surface oxygen vacancy formation and hydrogen adsorption, PCCP 16 (2014) 3036–3046, https://doi.org/10.1039/C3CP53991A.
[17] G. Hao, R. Zhang, J. Li, B. Wang, Q. Zhao, Insight into the effect of surface structure on H2 adsorption and activation over different CuO(111) surfaces: A first-principle study, Comput. Mater. Sci. 122 (2016) 191–200, https://doi.org/10.1016/j.commatsci.2016.05.023.
[18] X. Sun, D. Wu, W. Zhu, X. Chen, R. Sharma, J.C. Yang, G. Zhou, Atomic Origin of the Autocatalytic Reduction of Monoclinic CuO in a Hydrogen Atmosphere, J. Phys. Chem. Lett. (2021) 9547–9556, https://doi.org/10.1021/acs.jpclett.1c02369.
[19] C.R.A. Wright, A.P. Luff, E.H. Rennie, LII.—Third Report to the Chemical Society on "researches on some points in chemical dynamics", J. chem. Soc. Trans. 35 (1879) 475–524, https://doi.org/10.1039/CT8793500475.
[20] R.N. Pease, H.S. Taylor, The reduction of copper oxide by hydrogen, J. Am. Chem. Soc. 43 (1921) 2179–2188, https://doi.org/10.1021/ja01443a007.
[21] D. Jelić, B. Tomić-Tucaković, S. Mentus, A kinetic study of copper(II) oxide powder reduction with hydrogen, based on thermogravimetry, Thermochim Acta 521 (1-2) (2011) 211–217, https://doi.org/10.1016/j.tca.2011.04.026.
[22] K.C. Sabat, R.K. Paramguru, B.K. Mishra, Reduction of Copper Oxide by Low-Temperature Hydrogen Plasma, Plasma Chem. Plasma Process. 36 (2016) 1111–1124, https://doi.org/10.1007/s11090-016-9710-9.
[23] J. Pike, S.-W. Chan, F. Zhang, X. Wang, J. Hanson, Formation of stable Cu2O from reduction of CuO nanoparticles, Appl. Catal. A 303 (2) (2006) 273–277, https://doi.org/10.1016/j.apcata.2006.02.008.
[24] K.M. Shrestha, C.M. Sorensen, K.J. Klabunde, Synthesis of CuO Nanorods, Reduction of CuO into Cu Nanorods, and Diffuse Reflectance Measurements of CuO and Cu Nanomaterials in the Near Infrared Region, J. Phys. Chem. C 114 (2010) 14368–14376, https://doi.org/10.1021/jp103761h.
[25] L. Dorner, C. Cancellieri, B. Rheingans, M. Walter, R. Kagi, P. Schmutz, M. V. Kovalenko, L.P.H. Jeurgens, Cost-effective sol-gel synthesis of porous CuO nanoparticle aggregates with tunable specific surface area, Sci. Rep. 9 (2019) 13, https://doi.org/10.1038/s41598-019-48020-8.
[26] L. Dorner, P. Schmutz, R. Kagi, M.V. Kovalenko, L.P.H. Jeurgens, Electrophoretic Deposition of Nanoporous Oxide Coatings from Concentrated CuO Nanoparticle Dispersions, Langmuir 36 (2020) 8075–8085, https://doi.org/10.1021/acs.langmuir.0c00720.
[27] T. Ramanarayanan, J. Alonzo, Oxidation of copper and reduction of Cu 2 O in an environmental scanning electron microscope at 800° C, Oxid. Met. 24 (1985) 17–27.
[28] J. Li, J.W. Mayer, K.N. Tu, Nucleation and growth of Cu2O in the reduction of CuO thin films, Phys. Rev. B 45 (1992) 5683–5686, https://doi.org/10.1103/PhysRevB.45.5683.
[29] Y. Unutulmazsoy, C. Cancellieri, M. Chiodi, S. Siol, L. Lin, L.P.H. Jeurgens, In situ oxidation studies of Cu thin films: Growth kinetics and oxide phase evolution, J. Appl. Phys. 127 (2020) 065101, https://doi.org/10.1063/1.5131516.
[30] P. Willmott, D. Meister, S. Leake, M. Lange, A. Bergamaschi, M. Böge, M. Calvi, C. Cancellieri, N. Casati, A. Cervellino, The materials science beamline upgrade at the Swiss Light Source, J. Synchrotron Radiation 20 (2013) 667–682.
[31] G.K. White, Thermal expansion of cuprous oxide at low temperatures, J. Phys. C: Solid State Phys. 11 (11) (1978) 2171–2174, https://doi.org/10.1088/0022-3719/11/11/009.
[32] I.B. Krynetskiĭ, B.A. Gizhevskiĭ, S.V. Naumov, E.A. Kozlov, Size effect of the thermal expansion of nanostructural copper oxide, Phys. Solid State 50 (4) (2008) 756–758, https://doi.org/10.1134/S1063783408040264.
[33] Y. Unutulmazsoy, C. Cancellieri, M. Chiodi, S. Siol, L. Lin, L.P.H. Jeurgens, In situ oxidation studies of Cu thin films: Growth kinetics and oxide phase evolution, J. Appl. Phys. 127 (6) (2020) 065101, https://doi.org/10.1063/1.5131516.
[34] N.B. Pilling, R.E. Bedworth, The oxidation of metals at high temperatures, J. Inst. Met. 29 (1923) 529–582.

[35] R.M. German, Z.A. Munir, A correlation between the Pilling-Bedworth ratio and the radius of curvature of metallic substrates with coherent thin oxide layers, Oxid. Met. 8 (3) (1974) 123–129, https://doi.org/10.1007/BF00612168.
[36] H.J. Fan, U. Gösele, M. Zacharias, Formation of Nanotubes and Hollow Nanoparticles Based on Kirkendall and Diffusion Processes: A Review, Small 3 (10) (2007) 1660–1671, https://doi.org/10.1002/smll.200700382.
[37] Z. Grzesik, M. Migdalska, Oxidation Mechanism of Cu2O and Defect Structure of CuO at High Temperatures, High Temp. Mater. Processes (London) 30 (2011) 277–287, https://doi.org/10.1515/htmp.2011.046.
[38] J. Li, J. Mayer, Oxidation and reduction of copper oxide thin films, Mater. Chem. Phys. 32 (1992) 1–24.
[39] K. Mimura, J.-W. Lim, M. Isshiki, Y. Zhu, Q. Jiang, Brief review of oxidation kinetics of copper at 350 °C to 1050 °C, Metallur. Mater. Trans. A 37 (2006) 1231–1237, https://doi.org/10.1007/s11661-006-1074-y.
[40] B. Maack, N. Nilius, Morphological and Kinetic Insights into Cu 2 O–CuO Oxidation, Phys. Status Solidi B 257 (1) (2020) 1900365, https://doi.org/10.1002/pssb:v257.110.1002/pssb:201900365.
[41] P. Kofstad, Nonstoichiometry, diffusion, and electrical conductivity in binary metal oxides, (1972).
[42] R. Nakamura, D. Tokozakura, H. Nakajima, J.G. Lee, H. Mori, Hollow oxide formation by oxidation of Al and Cu nanoparticles, J. Appl. Phys. 101 (2007), 074303, https://doi.org/10.1063/1.2711383.
[43] R. Haugsrud, T. Norby, Determination of Thermodynamics and Kinetics of Point Defects in Cu2 O Using the Rosenburg Method, J. Electrochem. Soc. 146 (1999) 999–1004.
[44] A.E. Baber, F. Xu, F. Dvorak, K. Mudiyanselage, M. Soldemo, J. Weissenrieder, S. D. Senanayake, J.T. Sadowski, J.A. Rodriguez, V. Matolín, M.G. White, D. J. Stacchiola, In Situ Imaging of Cu2O under Reducing Conditions: Formation of Metallic Fronts by Mass Transfer, J. Am. Chem. Soc. 135 (2013) 16781–16784, https://doi.org/10.1021/ja408506y.
[45] R. Zhang, B. Wang, L. Ling, H. Liu, W. Huang, Adsorption and dissociation of H2 on the Cu2O(111) surface: A density functional theory study, Appl. Surf. Sci. 257 (4) (2010) 1175–1180, https://doi.org/10.1016/j.apsusc.2010.07.095.
[46] A. Ruiz Puigdollers, P. Schlexer, S. Tosoni, G. Pacchioni, Increasing Oxide Reducibility: The Role of Metal/Oxide Interfaces in the Formation of Oxygen Vacancies, ACS Catal. 7 (2017) 6493–6513, https://doi.org/10.1021/acscatal.7b01913.
[47] E. Chason, B.W. Sheldon, L.B. Freund, J.A. Floro, S.J. Hearne, Origin of Compressive Residual Stress in Polycrystalline Thin Films, Phys. Rev. Lett. 88 (2002) 156103, https://doi.org/10.1103/PhysRevLett.88.156103.
[48] J.A. Floro, S.J. Hearne, J.A. Hunter, P. Kotula, E. Chason, S.C. Seel, C.V. Thompson, The dynamic competition between stress generation and relaxation mechanisms during coalescence of Volmer-Weber thin films, J. Appl. Phys. 89 (2001) 4886–4897, https://doi.org/10.1063/1.1352563.
[49] S. Tajima, S. Tsuchiya, M. Matsumori, S. Nakatsuka, T. Ichiki, Reduction of Copper Oxide Films by an Atmospheric-Pressure Inductively Coupled Plasma Microjet, Trans. Mater. Res. Soc. Japan, 35 (2010) 621–625. http://doi.org/10.14723/tmrsj.35.621.
[50] S. Tajima, S. Tsuchiya, M. Matsumori, S. Nakatsuka, T. Ichiki, High-rate reduction of copper oxide using atmospheric-pressure inductively coupled plasma microjets, Thin Solid Films 519 (2011) 6773–6777, https://doi.org/10.1016/j.tsf.2011.01.219.
[51] J. Li, S.Q. Wang, J.W. Mayer, K.N. Tu, Oxygen-diffusion-induced phase boundary migration in copper oxide thin films, Phys. Rev. B 39 (1989) 12367–12370, https://doi.org/10.1103/PhysRevB.39.12367.